Published in final edited form as:
Nat Med. 2013 August ; 19(8): 1067–1072. doi:10.1038/nm.3252.

In vivo imaging of glucose uptake and metabolism in tumors

Simon Walker-Samuel[1], **Rajiv Ramasawmy**[1], **Francisco Torrealdea**[1,2], **Marilena Rega**[2], **Vineeth Rajkumar**[3], **S. Peter Johnson**[3], **Simon Richardson**[1], **Miguel Gonçalves**[1], **Harold G. Parkes**[4], **Erik Årstad**[5], **David L. Thomas**[2], **R. Barbara Pedley**[3], **Mark F. Lythgoe**[1,*], and **Xavier Golay**[2,*]

[1]UCL Centre for Advanced Biomedical Imaging, Division of Medicine and Institute of Child Health, London, UK

[2]UCL Institute of Neurology, London, UK

[3]UCL Cancer Institute, London, UK

[4]Cancer Research UK and EPRSC Cancer Imaging Centre, The Institute of Cancer Research and Royal Marsden NHS Foundation Trust, Sutton, Surrey, UK

[5]UCL Department of Chemistry, London, UK

Abstract

Tumors display a greater reliance on glycolysis for energy production than normal tissues. We have developed a non-invasive method for imaging glucose uptake *in vivo*, which is based on magnetic resonance imaging, and allows the uptake of non-labeled glucose to be measured via the chemical exchange of protons between hydroxyl groups and water. This method differs from existing molecular imaging methods, as it permits detection of the delivery and uptake of a metabolically active compound at physiological quantities. We show that our technique, named glucose chemical exchange saturation transfer (glucoCEST), is sensitive to tumor glucose accumulation in colorectal tumor models, and can distinguish tumor types with differing metabolic characteristics and pathophysiology. The results of this study suggest that glucoCEST has potential as a useful and cost-effective method for characterizing disease and assessing response to therapy in the clinic.

Corresponding Author: Simon Walker-Samuel, Address: Centre for Advanced Biomedical Imaging, University College London, Lower Ground Floor, Paul O'Gorman Building, 72 Huntley Street, London, WC1 6DD, Tel.: +44 20 7679 6329 simon.walkersamuel@ucl.ac.uk.
*MFL and XG jointly directed this research

Author contributions S.W-S designed and performed experiments, analysed data, developed the methodology and wrote the paper; R.R. performed glucose tail vein measurements, assisted with *in vivo* experiments and developed ASL post-processing software; F.T. and M.R. performed most phantom experiments and analysed data; P.J. and R.B.P. developed and set up tumor xenograft models; V.R. performed histology and autoradiography measurements, and analysed data; H.P. performed ^{13}C NMR experiments; S.R. designed bespoke apparatus for *in vivo* imaging; M.G. assisted with *in vivo* experiments; D.T., E.A., R.B.P., X.G. and M.L. gave conceptual advice and assisted in the design of experiments; X.G. devised the initial glucoCEST concept and experiment. X.G. and M.L jointly directed this research, helped perform experiments, and contributed to the writing and editing of this manuscript.

Competing Financial Interest Statement: I declare that the authors have no competing interests as defined by Nature Publishing Group, or other interests that might be perceived to influence the results and/or discussion reported in this paper.

Europe PMC Funders Author Manuscripts

Keywords

Biomarker; MRI; CEST; glucose; FDG; PET; tumor; imaging; metabolism; glycolysis

Introduction

Glucose is the primary source of energy in most organisms, where it is utilized in both aerobic and anaerobic respiration. Impaired or altered glucose consumption is associated with a range of pathological conditions, and the ability to non-invasively assess glucose uptake with [^{18}F]-flurodeoxyglucose (FDG) positron emission tomography (PET) has found wide clinical utility over the last 30 years. Here we propose a new way of detecting glucose uptake and metabolism, with no reliance on radiolabeled glucose analogues. Instead we use natural, non-radioactive glucose at physiologically reasonable quantities, which we image as it enters pathological tissues. Our technique is based on magnetic resonance imaging (MRI), which is a standard imaging modality available in most large hospitals, and it functions through a mechanism known as chemical exchange saturation transfer (CEST) [1].

Tumors display a greater reliance on glycolysis for energy production than normal tissues, a phenomenon known as the Warburg effect. This key discriminator of tumors from normal tissues, has been exploited as a target for anticancer therapy, as well in the detection of metastatic disease by FDG-PET [2]. The ability to probe tumor glucose uptake by MRI, without the use of radioactive tracers would offer significant cost reductions relative to FDG-PET, yet still provide important clinical benefits. With this in mind, we aimed in this study to evaluate the sensitivity of our technique (named glucoCEST [3,4]) to detect glucose uptake in tumors, and to compare it to standard markers of tumor metabolism and pathophysiology such as hypoxia and blood flow.

Results

Comparison of tumor glucoCEST measurements with [^{18}F]FDG autoradiography

GlucoCEST utilizes two properties of hydroxyl protons: first, when exposed to a magnetic field, the magnetic moments of hydroxyl protons precess at a different frequency to those of bulk tissue water, and can therefore be selectively labeled using radiofrequency pulses; second, hydroxyl and water protons undergo exchange, thereby allowing magnetic labeling to be transferred from glucose to water and for glucose to be detected from the change in water signal in MRI images (Fig. 1a) [1],. The CEST technique thus provides an amplification of detection by using the very large water signal, rather than relying on the much smaller signal from glucose.

Having determined *in vitro* that glucose concentrations of only a few millimolar could be detected with glucoCEST (Supplemental Fig. 1), we aimed to determine the potential for glucoCEST to measure regional glucose uptake *in vivo*. To this end, we performed a glucoCEST imaging experiment, which we compared 24 hours later with [^{18}F]FDG autoradiography. Two subcutaneous human colorectal tumor xenograft models were evaluated, LS174T and SW1222, with markedly different phenotypes [5].

In CEST experiments, the effect of exchangeable solute protons on the MRI water signal is visualized using the asymmetric magnetization transfer ratio (MTR_{sym}) curve. We here define a new parameter, the glucoCEST enhancement (GCE), as the change in the area under the MTR_{asym} curve from a baseline (Fig. 1b). Baseline images of the area under the MTR_{asym} curve reflect the influence of endogenous exchangeable protons [6], lipids [7] and other exchange processes on the water signal. These contaminating effects are removed by subtracting pre-injection from post-injection images, via the GCE parameter.

We used a gradient echo CEST (GE-CEST) sequence to acquire images from a slice through the largest axial extent of each tumor, at baseline and 60 minutes post-intraperitoneal (i.p.) bolus injection of glucose. A comparison of blood glucose measurements following i.p. and intravenous (i.v.) injections, and the subsequent glucoCEST response, suggested that the slow glucose kinetics following i.p. injection are preferable to the rapid changes following i.v. injection, with an increase in blood glucose concentration of approximately 5 mM (Supplemental Fig. 2). Images of glucose uptake from a cross-section through a mouse xenograft revealed a significantly greater GCE in SW1222 tumors compared with muscle (0.16 ± 0.04 and 0.04 ± 0.02 %, respectively, $P < 0.01$) (Fig. 2b).

Mice were returned to their cages and allowed to recover for 24 hours, after which between 10 and 15 MBq of [^{18}F]FDG was administered. Median activity at 60 minutes following administration was significantly higher in SW1222 than LS174T tumors ($P < 0.01$) (Fig. 3a). Similarly, we measured a significant difference in the median GCE in the two tumor types (Fig. 3b), and a statistically significant correlation between median [^{18}F]FDG and glucoCEST measurements ($r^2 = 0.70$, $P < 0.01$, Fig. 3c). [^{18}F]FDG and GCE images, both acquired at 60 minutes following injection, also displayed similar regional uptake (Fig.4).

The relationship between glucose uptake, perfusion and hypoxia

Composite fluorescence microscopy images of perfusion and hypoxia (Hoechst 33342 and pimonidazole, respectively) revealed SW1222 tumors to be more uniformly perfused and less hypoxic than LS174T tumors (5 ± 3 % and 35 ± 12 % hypoxia, respectively) (Fig. 4). We found no correlation between pimonidazole and Hoechst spatial distributions ($P > 0.05$). Pixel-by-pixel comparison of [^{18}F]FDG and pimonidazole uptake, following image registration and regridding, revealed a significant correlation in LS174T tumors ($P < 0.01$), but not in SW1222 tumors. No correlation was found, on a pixel-by-pixel basis, between Hoechst 33342 and FDG concentration, for either of the tumors.

Generally, pixel-by-pixel comparison of GCE and histological images was challenging due to non-linear deformations occurring during tissue processing, so averages from whole tumor sections were compared. From this analysis, GCE and pimonidazole uptake were correlated in LS174T tumors, but at a lower level of statistical significance ($P < 0.05$), and we found no correlation in the averaged signal from SW1222 tumors. No correlation was found between GCE and Hoechst uptake in either tumor type.

Compartmentalisation of tumor glucoCEST measurements

To investigate the relationship between the delivery of glucose to tumor tissue and its metabolism by tumor cells, we performed a glucoCEST experiment, immediately followed

by a dynamic contrast-enhanced (DCE) MRI acquisition, in which the uptake of a bolus of gadolinium-diethylenetriaminepentacetate (Gd-DTPA, a commonly used MRI contrast agent) was monitored with time as it is delivered to the tumor ($n = 4$ SW1222 and $n = 4$ LS174T tumors). Gd-DTPA is a useful marker of delivery as, following systemic injection, it extravasates into tissue via gaps in blood vessel walls, but cannot traverse cell membranes. Thus, a measurement of the uptake of Gd-DTPA in a tumor reflects the local blood flow, vascular permeability and volume of the extracellular space 8. Equally, the measured enhancement in a glucoCEST experiment could reflect each of these tissue properties, alongside an intracellular glucose fraction, potentially in a metabolized form (for example as hexoses and pentoses of the glycolytic pathway).

Comparison of images of the area under the curve (AUC) from DCE-MRI experiments, alongside GCE images showed some similarities between the regional uptake of Gd-DTPA and glucose (Supplemental Fig. 3), although the differences between the two measurements are arguably more apparent, and no significant correlation was found between them ($P > 0.05$).

In a further group of tumors ($n = 5$ SW1222 and $n = 5$ LS174T), we administered [U-^{13}C]glucose i.p. at the same dose as used in glucoCEST experiments. At 60 minutes following injection, tumors were freeze-clamped and resected. We acquired ^{1}H decoupled ^{13}C nuclear magnetic resonance (NMR) spectra of the aqueous phase separated from each tumor fragment (Fig. 5a). Glucose and glucose-6-phosphate were detected from doublets in the C1α region of ^{13}C spectra, with a relative chemical shift of 0.13 p.p.m. [9,10, 9,11]. The relative area of these peaks gave a ratio of labelled glucose-6-phosphate to glucose of 42 ± 18 % and 38 ± 21 % in SW1222 and LS174T tumors, respectively. In phantoms, glucose and glucose-6-phosphate produced similar z-spectra, whilst fructose-6-phosphate and fructose-6-biphosphate provided a smaller signal (Fig. 5b, Supplemental Fig. 4).

Also evident in ^{13}C spectra were lactate and amino acids such as glutamine, glutamate, taurine and alanine, resulting from the glutamine synthesis pathway. Interestingly, each of these amino acids contains amide groups that, *in vitro*, display a strong CEST effect from exchange between amide protons and water (Fig. 5c). Conversely, lactate, which was evident in ^{13}C spectra, shows a negligible CEST effect compared with glucose, with i*n vitro* measurements revealing a lactate area under the MTR_{asym} curve of 4% that of glucose. Similarly, the average CEST effect from glutamine, glutamate, taurine and alanine was 83 ± 5 % of that found in glucose, but centered on a single resonance at 3.5 p.p.m., compared with the three glucose resonances situated between 1 and 4 p.p.m.

Discussion

In this study, we presented a new technique named glucoCEST and used it to detect the uptake of exogenously administered, unlabeled glucose in tumors. Raised glucose uptake is a hallmark of solid tumors and its non-invasive assessment would be of key importance in the clinic, with potential applications including tumor detection, monitoring tumor progression and evaluating response to therapy. Whilst tumors were the focus of this study, it

is anticipated that glucoCEST could find utility in other conditions, such as Alzheimer's disease or stroke.

Our experiments revealed that glucoCEST was sufficiently sensitive to allow millimolar changes in tumor hydroxyl group concentration to be detected following injection. As glucoCEST measures the change in signal from baseline following glucose injection, endogenous levels of molecules with exchangeable protons (of either amide or hydroxyl groups) do not contribute to the glucoCEST effect and are assumed not to catalyze glucose-based hydroxyl proton exchange. However, bi-products of glucose metabolism following intracellular uptake of the administered glucose could contribute to the glucoCEST signal.

We compared glucoCEST with [^{18}F]FDG autoradiography, which provides a highly sensitive and specific measure of fluorodeoyglucose uptake. Whilst FDG is an analogue of glucose with slightly differing pharmacokinetics [12], it provides the closest gold-standard technique for comparison. In accordance with the result from glucoCEST experiments, [^{18}F]FDG autoradiography revealed a significantly lower uptake of glucose in LS174T than SW1222 tumors, and a marked spatial accordance was observed between FDG and glucose concentration maps. Moreover, median tumor GCE and FDG uptake values were significantly correlated, thereby providing a validation of the glucoCEST technique. These results also help inform on the compartmentalization of the signal measured using glucoCEST, as FDG can only be metabolized into its primary phosphorylated state, at which point it becomes 'trapped' in the cell. Due to the avid accumulation of glucose by tumor cells [13], a measurement at 60 minutes following administration is likely to contain a significant proportion of FDG that has accumulated in the intracellular compartment [14,15].

^{13}C NMR spectroscopy of tumor fragments administered [U-^{13}C]glucose revealed the presence of labeled glucose in both tumor types, which could be either intra- or extra-cellular in origin, alongside significant quantities of glucose-6-phosphate. Our *in vitro* measurements of the CEST effect caused by the first four molecular species in the glycolytic pathway show that intracellular stages of glycolysis can be detected with glucoCEST, with glucose-6-phosphate giving an approximately equal enhancement to glucose. The concentration of intracellular glucose has previously been found to depend strongly on the concentration of extracellular glucose, with one study estimating the intracellular glucose concentration to be half of that outside the cell [16]. Similarly, John *et al.* [17] showed that the level of intracellular glucose depends on the rate of glucose uptake and metabolism, which in turn depends on cell type, with intracellular glucose ranging from very low (< 0.07 mM) to levels as high as those of extracellular glucose (> 5 mM).

Thus, whilst neither 13C NMR nor glucoCEST can distinguish between intra- and extracellular free glucose, a contribution by intracellular glucose to the glucoCEST signal is possible, and an attenuation of the signal from extracellular glucose could occur due to the lower pH of the extracellular fluid. Indeed, from phantom measurements (Supplemental Fig. 5), an intracellular and extracellular pH of 7.2 and 6.9, respectively, could result in a 16% lower signal from the extracellular compartment, per mole of glucose. These data, together with the lack of spatial concordance with Gd-DTPA-enhanced maps suggest that glucoCEST

is not simply reporting on vascular delivery of glucose, but also on cellular uptake and metabolic activity.

[U-^{13}C] glucose NMR also revealed the incorporation of glucose carbon molecules into amino acids such as glycine, glutamine, taurine and alanine. Under the assumption that the presence of additional glucose causes an increase in the concentration of these molecules, the large CEST effect associated with these molecules from amide proton exchange (rather than hydroxyl proton exchange) [18,19] could provide an alternative intracellular contribution to the glucoCEST signal. It is conceivable that the differing shapes of z-spectra associated with hydroxyl and amide proton exchange may allow these two phenomena to be modeled and separated *in vivo*, which would potentially allow glycolysis and glutamine synthesis and metabolism to be separately probed. Thus, the combined effects of 1) extended vascular delivery of glucose, 2) the presence of extracellular glucose, intracellular glucose and phosphorylated sugars in the glycolytic pathway, 3) increases in amino acid concentration from glutamine synthesis and 4) a lower extracellular pH, lead to the conclusion that the source of the glucoCEST signal could be attributed to both intra- and extra-cellular compartments, which explains its accordance with [^{18}F]FDG autoradiography measurements.

A correspondence was also found with pimonidazole staining for hypoxia in LS174T tumors, which agrees with previous measurements in the same model by Dearling *et al.*, who showed that this was due to the expression of glucose transporters GLUT-1 and GLUT-4 [20]. We did not find this relationship in SW1222 tumors, which were much less hypoxic. It is also important to note that the lack of correlation between either FDG or glucoCEST signal and Hoechst 33342 staining (a measure of perfusion), which would indicate that the measured glucoCEST signal is not limited by vascular delivery, as also argued above in relation to Gd-DTPA uptake. This result is particularly relevant as the glucoCEST signal is potentially sensitive to physiological changes induced by hyperglycemia, such as increased blood flow and decreased pH. Additional measurements of both properties following glucose injection showed that neither blood flow nor pH changed for the dose of glucose administered (1.1 mmol kg^{-1}), thereby confirming that the observed glucoCEST signal was not caused by concomitant effects due to hyperglycemia (defined as a blood glucose concentration of greater than 20 mM [21]) (Supplemental Fig. 6).

The major findings of this study are therefore: 1) glucoCEST has the sensitivity to discriminate between differing tumor phenotypes, and 2) that glucoCEST and [^{18}F]FDG may be able to provide similar, yet complimentary information. These conclusions have strong implications for future utility of glucoCEST, as the ability to discriminate between tumors of differing pathophysiology, would be of particular utility for diagnosis, prognosis and potentially for assessing response to therapy.

Some challenges associated with clinical translation of the glucoCEST remain to be overcome, such as the lower field strengths used in the clinic, which will reduce the chemical shift between glucose and water and thereby increase the coalescence time, during which the chemical exchange rate will be faster than the chemical shift. However, the effect of this difference on the glucoCEST signal is not straightforward to predict, and must be

experimentally evaluated on clinical systems. The potential loss of contrast-to-noise ratio caused by lower field strengths may in part be compensated by the advanced, rapid imaging technologies available on clinical scanners. Whilst no clinical implementations of accelerated CEST acquisition schemes have yet been reported, techniques such as echo-planar imaging, steady state free precession and fast spin echo have been extensively used in magnetization transfer imaging, which is a closely related technique, and could be readily applied to a CEST measurement [22-24]. Similarly, as glucoCEST relies on the measurement of sufficient contrast between signals from different selective saturations, signal averaging, in conjunction with rapid imaging techniques, would enable such differences to be more easily discriminated within a clinically acceptable examination time.

If sufficiently sensitive, glucoCEST offers a promising new tool for probing tumor glucose accumulation and metabolism, which naturally aligns FDG-PET as an obvious candidate for comparison. Whilst FDG-PET uses trace levels of flurodeoxyglucose, we have shown that the physiological levels of glucose required for detection by glucoCEST are insufficient to produce any measurable changes in pH or blood flow. Scaling the dose used in this study to a 70 kg human corresponds to 14 g of glucose, which is approximately the same as found in half a standard sized chocolate bar. Oral administration could induce a greater insulin response than i.p. injection [25], but would be easier to implement in the clinic than i.v. injection and would more closely mimic the slow enhancement protocol investigated in this study. A drinkable sugar solution could conceivably be ingested whilst in the scanner, similar to that used in standard glucose tolerance testing in diabetes patients [26], which would enhance patient acceptance, although a period of fasting prior to the scan may also be required in order to stabilize baseline blood glucose, as is commonly performed with a range of medical examinations [27,28].

GlucoCEST could thus offer a viable alternative to FDG-PET, particularly as [^{18}F]FDG is expensive to manufacture and necessarily has an associated radiation dose, which limits the ability to perform repeated, longitudinal measurements and can prohibit examination of certain patient populations (such as young children and pregnant women [27,28]). Equally, as glucoCEST uses simple, unlabeled glucose to provide image contrast, the logistics and infrastructure necessary for the production and delivery of [^{18}F]-FDG are removed, thereby simplifying the imaging procedure. FDG-PET is generally considered to be more expensive than MRI [29,30], so glucoCEST could also offer considerable financial savings (although estimated costs for the two modalities can vary substantially from country to country [31]). Furthermore, as the resolution of modern PET systems (typically of the order of 5×5×5 mm^3 [32]) is much lower than

Methods

Tumor models

All *in vivo* experiments were performed in accordance with the UK Home Office Animals Scientific Procedures Act, 1986 and UKCCCR guidelines [33]. 5×10^6 LS174T or SW1222 human colorectal carcinoma cells were injected subcutaneously into the right flank of female MF1 *nu*/*nu* mice using a 27G needle and allowed to grow for 10 to 16 days.

GlucoCEST magnetic resonance imaging experiments

We acquired all MRI data using a horizontal bore 9.4 T VNMRS system (Agilent, Oxford, UK). Prior to imaging, mice were fasted for 24 hours and anaesthetized in an induction box using 3% isoflurane in oxygen, followed by 1.5% via a nose cone during MRI. Core body temperature was monitored and maintained using physiological monitoring apparatus and a warm air blower. A solution of glucose was prepared in saline at a concentration of 140 mM, and 0.2 mL and administered as a bolus, i.v. via a tail vein or i.p., using a non-metallic pediatric cannula and a line running through the MRI scanner.

Tumors were localized using a T_2-weighted fast spin echo sequence (see Supplemental Methods). From which we defined a slice through the largest extent of the tumor to use in subsequent imaging measurements. GlucoCEST data were acquired using either a gradient-echo CEST (GE-CEST) imaging sequence or an exchange-modulated point resolved spectroscopy (EXPRESS) sequence for single voxel (whole-tumour) measurements [34]. In the GE-CEST acquisition, lines from each image were acquired in a linear order, such that, for 128 phase-encoding steps, 100 saturation pulses were applied within the outer third of k-space, enabling a steady-state to be reached (Supplemental Fig. 7). Data post-processing involved the conversion of signal intensity data to the asymmetric magnetization transfer (MTR_{asym}), and the glucoCEST enhancement (GCE), defined as the change in the area under the MTRasym curve between 0.75 and 4 p.p.m.

Arterial spin labeling

We acquired ASL data using a FAIR Look-Locker sequence with a single-slice spoiled gradient echo readout [35]. Perfusion maps were calculated [36] by assuming a blood-partition constant of 0.9 and longitudinal relaxation time of blood of 1900 ms [37].

Dynamic contrast-enhanced MRI

Mice were administered a 50 mM solution of Gd-DTPA (Magnevist, Schering, Berlin) in saline as a bolus, i.p. (0.2 mmol kg^{-1}). Prior to injection, we estimated the the baseline longitudinal relaxation rate by fitting a three parameter model to multiple inversion recovery Look-Locker data. Gradient echo image data were acquired for 5 minutes to measure baseline signal intensity, and then for another 60 minutes following injection of contrast agent. The area under the gadolinium curve (AUC) was then calculated.

[^{18}F]-flurodeoxyglucose (FDG) autoradiography

Between 10 and 15 MBq of [^{18}F]FDG was administered i.p. in 0.3 mL of saline. [^{18}F]FDG was allowed to circulate for 60 minutes to mirror glucoCEST experiments, at which point tumors were rapidly excised. We maintained the orientation of the tumor and, following excision, tumors were snap-frozen using liquid nitrogen-cooled isopentane and cut in half along the longest axial diameter, corresponding to the MRI imaging slice. Standard curves for quantification of [^{18}F]FDG activity were produced by spotting serial dilutions of the administered dose (1, 0.1, 0.01 and 0.001%).

Europe PMC Funders Author Manuscripts

[U-^{13}C]glucose nuclear magnetic resonance spectroscopy of tumor fragments

[U-^{13}C]glucose (Sigma-Aldrich, Gillingham, UK) was administered i.p. to mice, following the *in vivo* glucoCEST protocol on the benchtop. At 60 minutes following injection, tumors were freeze-clamped, resected and stored at −80 °C. Samples were separated into aqueous and organic phases (see Supplementary Methods), freeze-dried, and ^{1}H-decoupled ^{13}C NMR spectra of the aqueous phase acquired using a 500 MHz Bruker DRX spectrometer (Bruker, Karlsruhe, Germany). ^{13}C free induction decays were processed with a 3 Hz line broadening prior to Fourier transform. Spectra were analysed using MestReC (Mestrelab, Santiago de Compostela, Spain) and in-house software written in the Interactive Data Language (IDL, Boulder, California), to fit multiple Lorentzian lineshapes.

Immunofluorescence and Histochemical Analysis

Pimonidazole was administered i.p. (60 mg kg^{-1}) and allowed to circulate for 30 minutes prior to sacrifice in order to measure tumor hypoxia with fluorescence microscopy. Hoechst 33342 was administered i.v. (10 mg kg^{-1}) and allowed to circulate for 3 minutes before tumors were rapidly resected, cut in half, and one half snap-frozen in isopentane cooled with liquid nitrogen; the other half was fixed in formaldehyde. Frozen tumor tissue was sectioned at 10 μm, with tumor orientation maintained for comparison with MRI scans. Sections were viewed using an Axioimager microscope (Carl Zeiss, UK) at x10 magnification. Perfusion was viewed by a UV filter (365 nm excitation), and hypoxia by a FITC filter (450 – 490 nm excitation). The percentage tumor hypoxia and perfusion were quantified by defining autofluoresence thresholds [38,39].

Statistical analysis

The Mann-Whitney U test was used throughout to assess differences in the magnitude of samples from two measurements; Spearman's rho was used to assess correlation. A *P*-value of less than 0.05 was taken to imply significance.

Supplementary Material

Refer to Web version on PubMed Central for supplementary material.

Acknowledgements

King's College London and UCL Comprehensive Cancer Imaging Centre CR-UK & EPSRC, in association with the MRC and DoH (England), and the British Heart Foundation.

Grant Information: Cancer Research UK and the Engineering and Physical Sciences Research Council (EPSRC) Cancer Imaging Centre in association with the Medical Research Council (MRC) and the Department of Health (England) (C1060/A10334), Cancer Research UK (C1519/A10331, C16412/A6269 and C309/A8274)

References

1. Ward KM, Balaban RS. Determination of pH using water protons and chemical exchange dependent saturation transfer (CEST). Magn Reson Med. 2000; 44:799–802. [PubMed: 11064415]
2. Kelloff GJ, et al. Progress and promise of FDG-PET imaging for cancer patient management and oncologic drug development. Clin Cancer Res. 2005; 11:2785–2808. [PubMed: 15837727]

Europe PMC Funders Author Manuscripts

3. Chan, KW., et al. International Society for Magnetic Resonance in Medicine. Montreal: 2011. Imaging of glucose uptake in breast tumors using non-labeled D-glucose.
4. Walker-Samuel, S., Johnson, SP., Pedley, RB., Lythgoe, MF., Golay, X. International Society for Magnetic Resonance in Medicine. Montreal: 2011. Assessment of tumour glucose uptake using gluco-CEST.
5. El Emir E, et al. Predicting response to radioimmunotherapy from the tumor microenvironment of colorectal carcinomas. Cancer research. 2007; 67:11896–11905. [PubMed: 18089820]
6. Zhou J, Wilson DA, Sun PZ, Klaus JA, Van Zijl PC. Quantitative description of proton exchange processes between water and endogenous and exogenous agents for WEX, CEST, and APT experiments. Magn Reson Med. 2004; 51:945–952. [PubMed: 15122676]
7. Walker-Samuel S, Peter Johnson S, Pedley B, Lythgoe MF, Golay X. Extracranial measurements of amide proton transfer using exchange-modulated point-resolved spectroscopy (EXPRESS). NMR Biomed. 2011
8. Walker-Samuel S, Leach MO, Collins DJ. Evaluation of response to treatment using DCE-MRI: the relationship between initial area under the gadolinium curve (IAUGC) and quantitative pharmacokinetic analysis. Physics in medicine and biology. 2006; 51:3593–3602. [PubMed: 16825751]
9. Ugurbil K, Brown TR, den Hollander JA, Glynn P, Shulman RG. High-resolution 13C nuclear magnetic resonance studies of glucose metabolism in Escherichia coli. Proceedings of the National Academy of Sciences of the United States of America. 1978; 75:3742–3746. [PubMed: 358201]
10. Kalderon B, Korman SH, Gutman A, Lapidot A. Estimation of glucose carbon recycling in children with glycogen storage disease: A 13C NMR study using [U-13C]glucose. Proceedings of the National Academy of Sciences of the United States of America. 1989; 86:4690–4694. [PubMed: 2734314]
11. Kunnecke B, Kustermann E, Seelig J. Simultaneous in vivo monitoring of hepatic glucose and glucose-6-phosphate by (13)C-NMR spectroscopy. Magn Reson Med. 2000; 44:556–562. [PubMed: 11025511]
12. Hariharan R, et al. Fundamental limitations of [18F]2-deoxy-2-fluoro-D-glucose for assessing myocardial glucose uptake. Circulation. 1995; 91:2435–2444. [PubMed: 7729031]
13. Hanahan D, Weinberg RA. The hallmarks of cancer. Cell. 2000; 100:57–70. [PubMed: 10647931]
14. Eary JF, Mankoff DA. Tumor metabolic rates in sarcoma using FDG PET. J Nucl Med. 1998; 39:250–254. [PubMed: 9476930]
15. Zaidi, H. Quantitative Analysis in Nuclear Medicine Imaging. 2005.
16. Fehr M, Lalonde S, Lager I, Wolff MW, Frommer WB. In vivo imaging of the dynamics of glucose uptake in the cytosol of COS-7 cells by fluorescent nanosensors. J Biol Chem. 2003; 278:19127–19133. [PubMed: 12649277]
17. John SA, Ottolia M, Weiss JN, Ribalet B. Dynamic modulation of intracellular glucose imaged in single cells using a FRET-based glucose nanosensor. Pflugers Archiv : European journal of physiology. 2008; 456:307–322. [PubMed: 18071748]
18. Zhou J, Lal B, Wilson DA, Laterra J, van Zijl PC. Amide proton transfer (APT) contrast for imaging of brain tumors. Magn Reson Med. 2003; 50:1120–1126. [PubMed: 14648559]
19. Zhou J, Payen JF, Wilson DA, Traystman RJ, van Zijl PC. Using the amide proton signals of intracellular proteins and peptides to detect pH effects in MRI. Nature medicine. 2003; 9:1085–1090.
20. Dearling JL, et al. Analysis of the regional uptake of radiolabeled deoxyglucose analogs in human tumor xenografts. J Nucl Med. 2004; 45:101–107. [PubMed: 14734681]
21. Walker-Samuel S, et al. Improving apparent diffusion coefficient estimates and elucidating tumour heterogeneity using Bayesian adaptive smoothing. Magnetic Resonance in Medicine. 2011; 65
22. Gloor M, Scheffler K, Bieri O. Intrascanner and interscanner variability of magnetization transfer-sensitized balanced steady-state free precession imaging. Magn Reson Med. 2011; 65:1112–1117. [PubMed: 21413076]
23. Ranjeva JP, Franconi JM, Manelfe C, Berry I. Magnetization transfer with echo planar imaging. MAGMA. 1997; 5:259–265. [PubMed: 9440826]

24. Tyler DJ, Gowland PA. Rapid quantitation of magnetization transfer using pulsed off-resonance irradiation and echo planar imaging. Magn Reson Med. 2005; 53:103–109. [PubMed: 15690508]
25. Andrikopoulos S, Blair AR, Deluca N, Fam BC, Proietto J. Evaluating the glucose tolerance test in mice. Am J Physiol Endocrinol Metab. 2008; 295:E1323–1332. [PubMed: 18812462]
26. Alberti KG, Zimmet PZ. Definition, diagnosis and classification of diabetes mellitus and its complications. Part 1: diagnosis and classification of diabetes mellitus provisional report of a WHO consultation. Diabet Med. 1998; 15:539–553. [PubMed: 9686693]
27. Delbeke D, et al. Procedure guideline for tumor imaging with 18F-FDG PET/CT 1.0. J Nucl Med. 2006; 47:885–895. [PubMed: 16644760]
28. Parker JA, Yester MV, Daube-Witherspoon E, Todd-Pokropek AE, Royal HJ. Procedure guideline for general imaging: 1.0. Society of Nuclear Medicine. J Nucl Med. 1996; 37:2087–2092. [PubMed: 8970540]
29. Shortt CP, et al. Whole-Body MRI versus PET in assessment of multiple myeloma disease activity. AJR Am J Roentgenol. 2009; 192:980–986. [PubMed: 19304704]
30. Plathow C, et al. Cost considerations for whole-body MRI and PET/CT as part of oncologic staging. Der Radiologe. 2008; 48:384–396. [PubMed: 17891370]
31. Antoch G, et al. Whole-body dual-modality PET/CT and whole-body MRI for tumor staging in oncology. JAMA. 2003; 290:3199–3206. [PubMed: 14693872]
32. Vallabhajosula, S. Molecular Imaging: Radiopharmaceuticals for PET and SPECT. Springer; London: 2009.
33. Workman P, et al. Guidelines for the welfare and use of animals in cancer research. Br J Cancer. 2010; 102:1555–1577. [PubMed: 20502460]
34. Walker-Samuel S, Johnson SP, Pedley B, Lythgoe MF, Golay X. Extracranial measurements of amide proton transfer using exchange-modulated point-resolved spectroscopy (EXPRESS). NMR Biomed. 2012; 25:829–834. [PubMed: 22135248]
35. Campbell-Washburn AE, et al. Cardiac arterial spin labeling using segmented ECG-gated Look-Locker FAIR: Variability and repeatability in preclinical studies. Magn Reson Med. 2012
36. Belle V, et al. In vivo quantitative mapping of cardiac perfusion in rats using a noninvasive MR spin-labeling method. J Magn Reson Imaging. 1998; 8:1240–1245. [PubMed: 9848735]
37. Campbell AE, et al. Equilibrium contrast CMR for the detection of amyloidosis in mice. Journal of Cardiovascular Magnetic Resonance. 2011; 13:O60.
38. Walker-Samuel S, et al. Non-invasive in vivo imaging of vessel calibre in orthotopic prostate tumour xenografts. International journal of cancer. 2012; 130:1284–1293. [PubMed: 21469141]
39. Burrell JS, et al. Investigating temporal fluctuations in tumor vasculature with combined carbogen and ultrasmall superparamagnetic iron oxide particle (CUSPIO) imaging. Magn Reson Med. 2011; 66:227–234. [PubMed: 21305600]

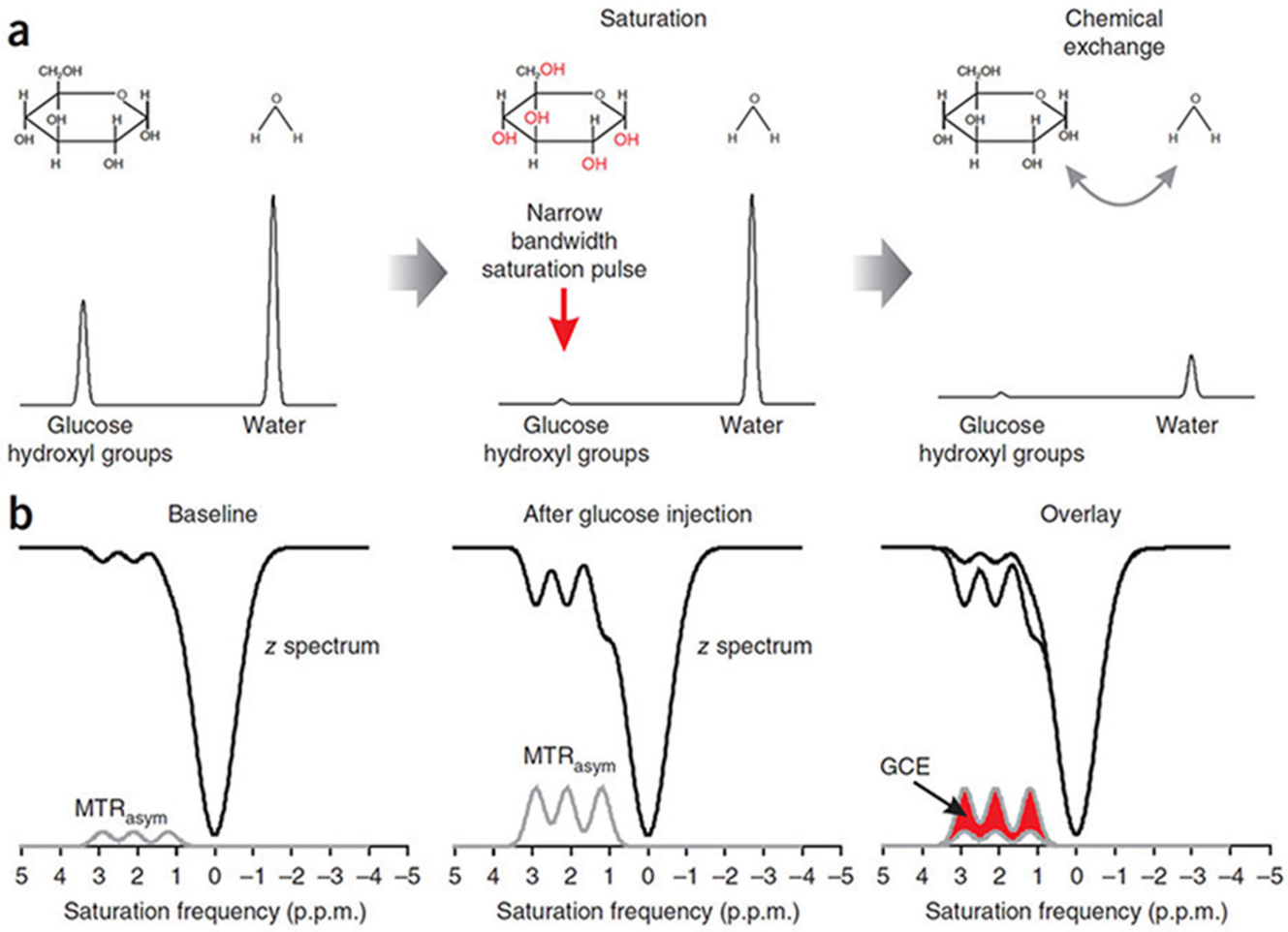

Figure 1.

a) Schematic diagram illustrating the principles underlying glucoCEST, showing simulated magnetic resonance frequency spectra with a single glucose (hydroxyl group) and water peak (not to scale). Glucose and water pools with full equilibrium magnetisation are irradiated with a narrow bandwidth radiofrequency pulse, centred at the hydroxyl group resonant frequency, which saturates their magnetisation. Protons in hydroxyl groups then exchange with water protons, transferring their magnetisation, and reducing the signal that can be measured. By continuously saturating the signal from water through this exchange process, thereby further reducing the large water signal, glucoCEST provides an amplification process for the glucose signal. b) In a CEST experiment, the water signal is usually measured as a function of saturation pulse frequency, which is known as the z-spectrum. Simulated z-spectra are shown here, with three hydroxyl group resonances, alongside the asymmetric magnetisation transfer ratio (MTR_{asym}, the difference in signal either side of the water peak centred at 0 p.p.m.). Following glucose injection, the concentration of hydroxyl groups resonating at 1.2, 2.1 and 2.9 p.p.m. from water increases, causing an increase in the size of the hydroxyl peaks in the MTRasym spectrum. The glucoCEST enhancement (GCE) is defined as the change in the area under the MTR_{asym}

curve from baseline. (Note that, for simplicity, only the effect of glucose and not of metabolic products of glycolysis are shown.)

Europe PMC Funders Author Manuscripts

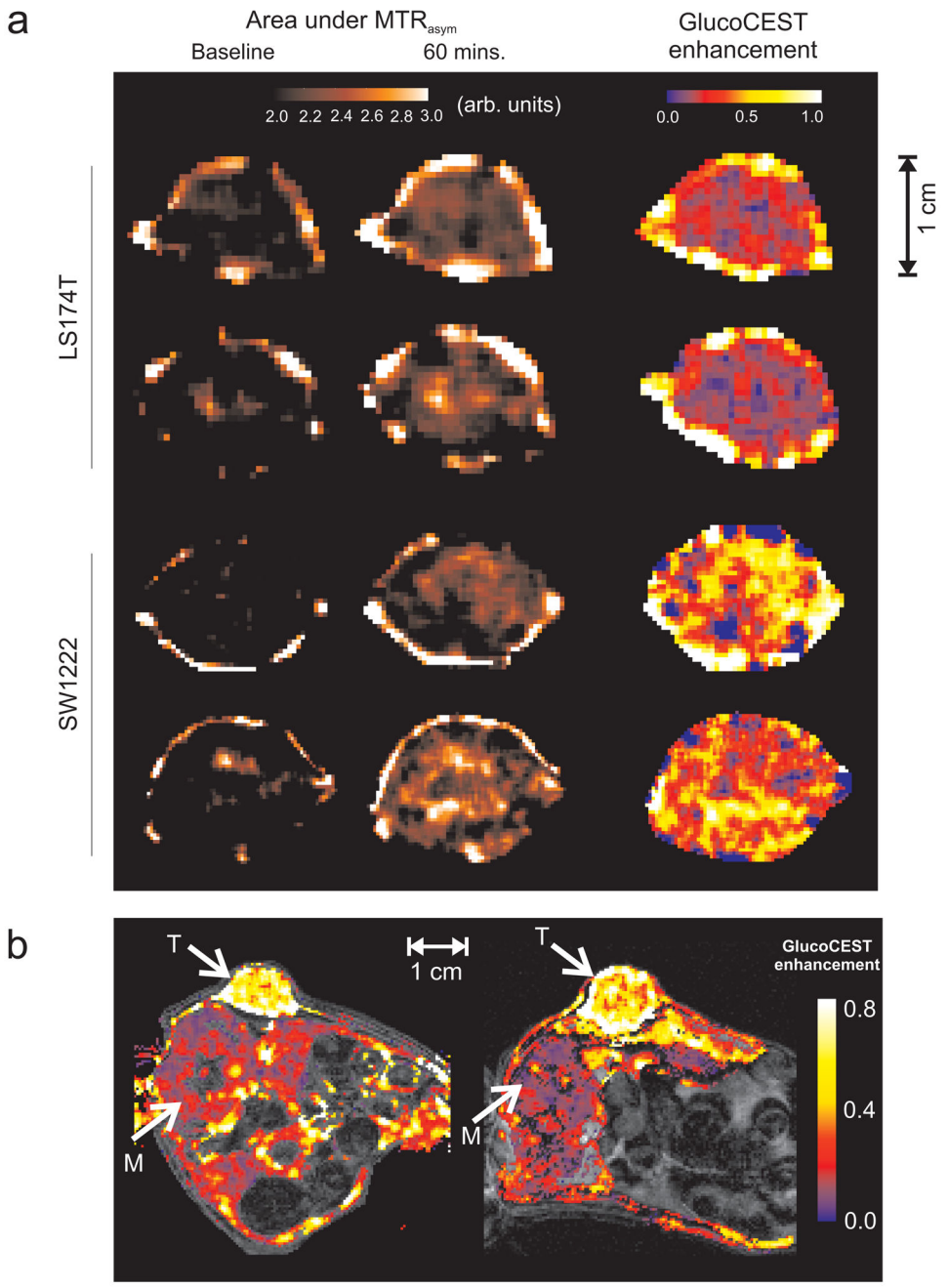

Figure 2.

a) Example glucoCEST image data from four tumors, showing raw, area under the MTRasym images pre- and 60 minutes post-injection of 1.1 mmol kg^{-1} glucose solution. Images from two types of human colorectal tumor xenograft models with differing vascular and cellular phenotypes (LS174T and SW1222) are shown. Baseline image contrast reflects variations in water content, endogenous exchangeable protons, lipid signal and conventional magnetisation transfer effects. Also displayed are the corresponding glucoCEST enhancement (GCE) images, which show the change in MTR$_{asym}$ at 60 minutes following

glucose injection. b) GCE maps from a cross-section through two mouse xenografts (SW1222), with tumour (T) and paraspinal muscle (M) regions highlighted with arrows. The colour scale represents GCE, whilst underlying greyscale images are for anatomical reference; regions subject to motion during the acquisition (e.g. gut) have been removed from glucose images for clarity. Glucose uptake in the tumour is visibly higher than in the muscle. All data were acquired using the GE-CEST sequence.

Europe PMC Funders Author Manuscripts

Europe PMC Funders Author Manuscripts

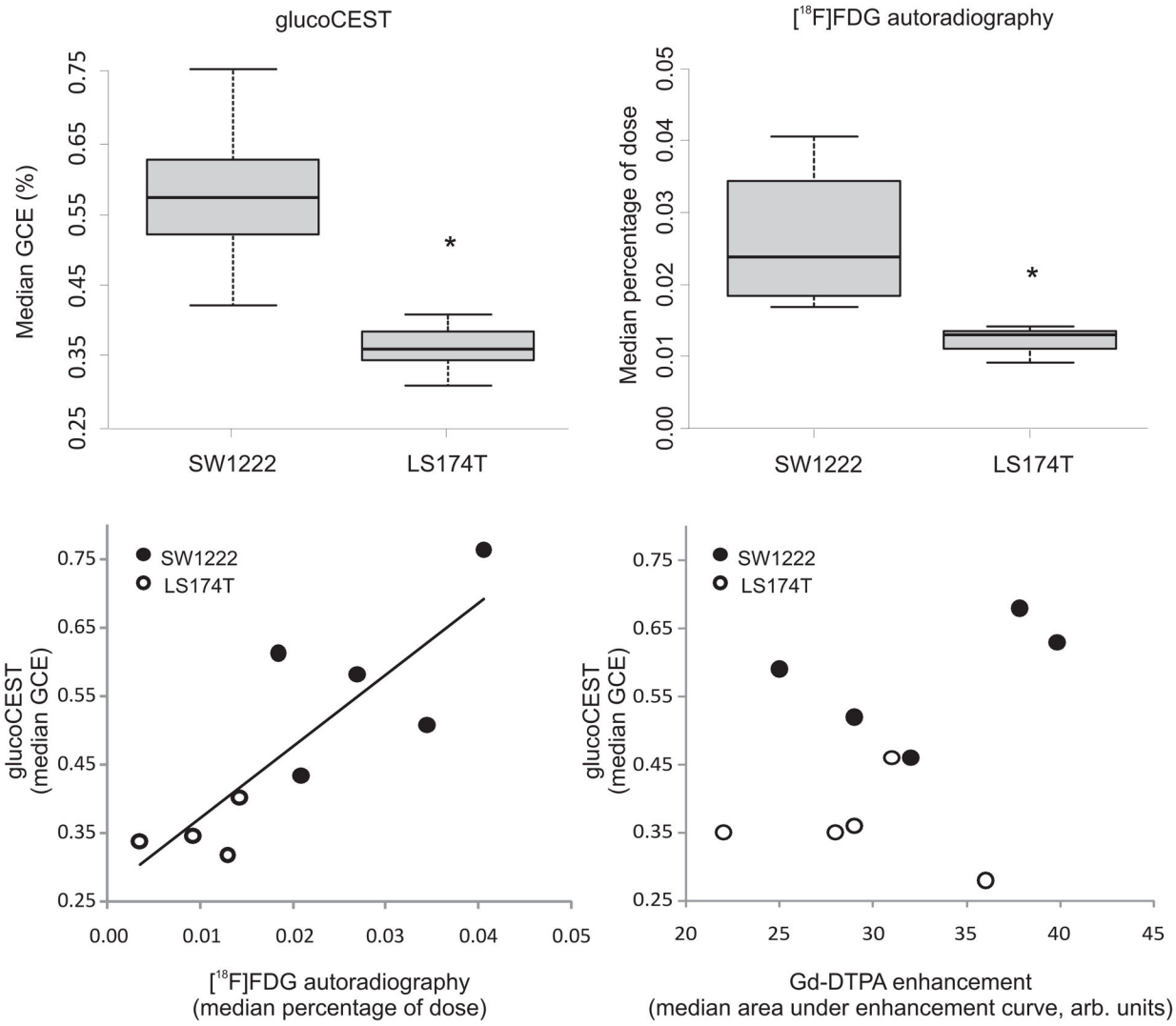

Figure 3.

Tumor glucose uptake measured using glucoCEST (a) and [^{18}F]FDG autoradiography (b) in two human colorectal tumor xenograft models (SW1222 and LS174T). Uptake of both glucose and FDG was significantly different between tumor types (*, $P < 0.01$, Mann-Whitney). The central bar in panels a and b shows the mean value, the edges of the box represent quartile values, and the whiskers show the upper and lower range. (c) Scatter plot of median tumor [^{18}F]FDG and glucoCEST enhancement, which shows a significant correlation ($P < 0.01$, Spearman's rho). (d) Scatter plot of median Gd-DTPA and glucoCEST enhancement, which are not significantly correlated ($P > 0.05$, Spearman's rho). All CEST data were acquired using the GE-CEST sequence.

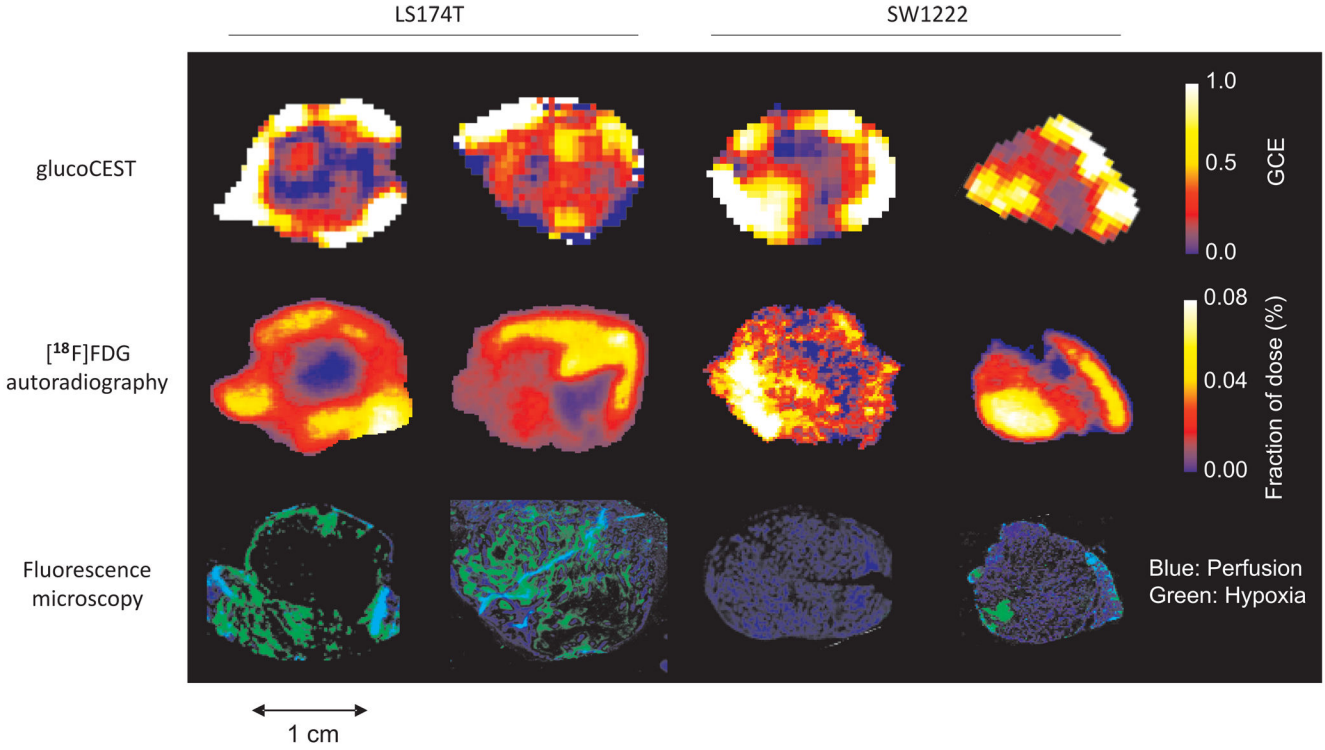

Figure 4.

Example glucoCEST, [^{18}F]FDG autoradiography and fluorescence microscopy images, obtained from the same tumor section (two LS174T and two SW1222 human colorectal xenograft models). Fluorescence microscopy images show perfused (blue) and hypoxic regions (green) corresponding to Hoechst 33342 and pimonidazole staining, respectively. All CEST data in this figure were acquired using the GE-CEST sequence.

Europe PMC Funders Author Manuscripts

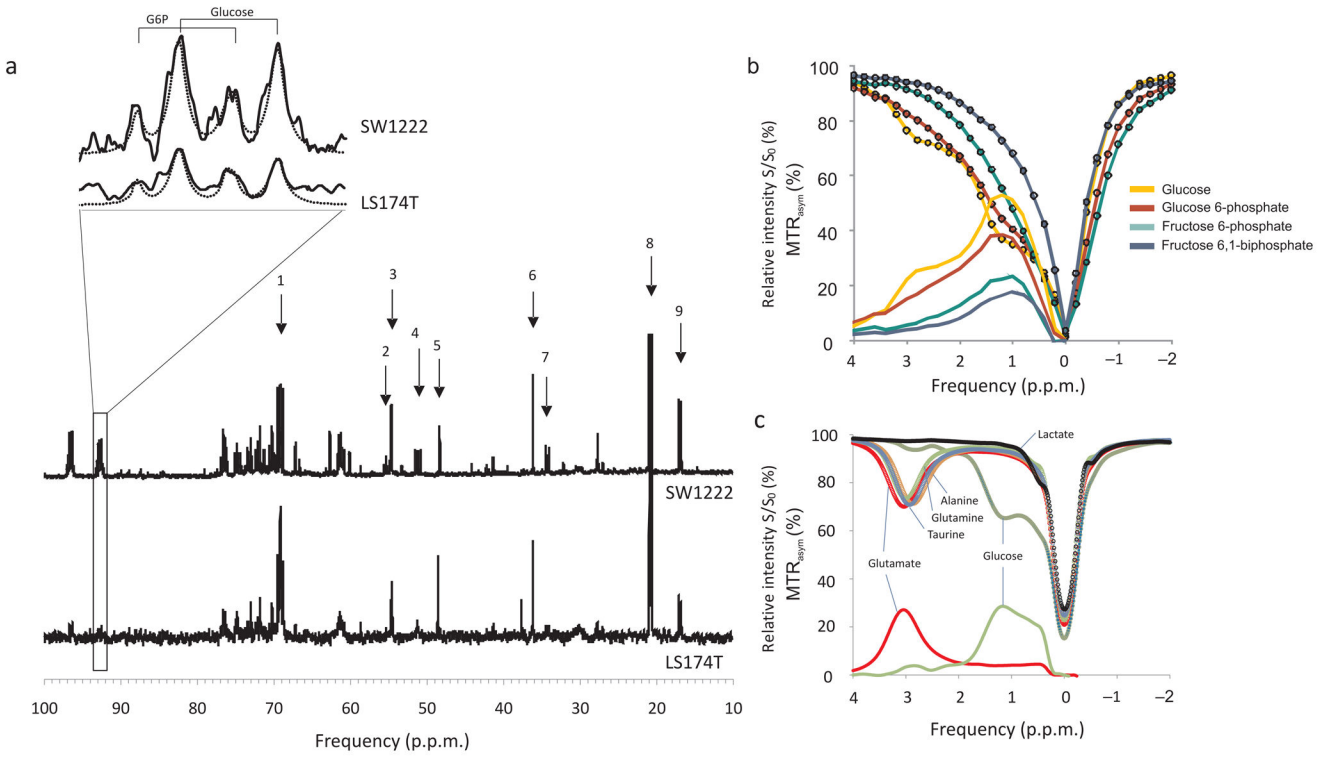

Figure 5.

a) Example ^{1}H decoupled ^{13}C NMR spectra from SW1222 and LS174T tumors that were administered [U-^{13}C]glucose, following the protocol for glucoCEST experiments. Peak assignments are: 1, lactate C2; 2, glutamate C2; 3, glutamine C2; 4, alanine C2; 5, taurine C1; 6, taurine C2; 7, glutamate C4; 8, lactate C3; 9, alanine C3. An expansion of the C1α multiplet is shown, corresponding to doublets from glucose and glucose-6-phosphate, (chemically shifted by 0.13 p.p.m. from the glucose doublet). Fitted Lorentzian peaks are overlaid overlaid. b) Z- and MTR_{asym} spectra from glucose, glucose 6-phosphate, fructose 6-phosphate and fructose 6,1-biphosphate. *In vitro*, glucose and glucose-6-phosphate display similar CEST effects, whilst fructose-6-phosphate and fructose 6,1-biphosphate show a smaller effect (Supplemental Fig. 4). c) Z- and MTR_{asym} spectra from glucose, lactate, glutamine, glutamate, alanine and taurine. Glucose displays a strong CEST effect from to hydroxyl proton exchange, whilst the amino acids show a CEST effect via amide proton exchange; lactate shows a minimal effect.